Search for lepton-flavour-violating decays of the Z boson into a τ-lepton and a light lepton with the ATLAS detector

W. S. Chan[1], on behalf of the ATLAS collaboration

1 Nikhef National Institute for Subatomic Physics, Amsterdam; Netherlands.
* ws.chan@cern.ch

December 6, 2018

Proceedings for the 15th International Workshop on Tau Lepton Physics,
Amsterdam, The Netherlands, 24-28 September 2018
scipost.org/SciPostPhysProc.Tau2018

Abstract

Lepton flavour violation in the charged lepton sector is an unambiguous signal of physics beyond the Standard Model. Searches for lepton flavour violation in decays of the Z boson with the ATLAS detector is reported, focusing on decays into an electron or muon and a hadronically decaying τ-lepton, using pp collisions data with a centre-of-mass energy of 13 TeV. Upper limits on the branching ratios of lepton-flavor-violating decays are set at the 95% confidence level: $\mathcal{B}(Z \to e\tau) < 5.8 \times 10^{-5}$ and $\mathcal{B}(Z \to \mu\tau) < 2.4 \times 10^{-5}$. When combined with a previous ATLAS result based on pp collisions data with a centre-of-mass energy of 8 TeV, an upper limit of $\mathcal{B}(Z \to \mu\tau) < 1.3 \times 10^{-5}$ is obtained.

1 Introduction

In the Standard Model (SM), flavour is not a conserved global symmetry in general. It is well known that flavour-changing processes exist in the quark and neutrino sectors. These processes can be described by the CKM quark-mixing matrix and the PMNS neutrino-mixing matrix. However, the mixing of charged leptons have not yet been observed so far. In the SM, lepton-flavour-violating (LFV) processes such as $Z \to \mu\tau$ are possible beyond tree level with neutrino oscillations considered (Fig. 1), but with vanishingly small branching ratios ($\sim 10^{-54}$) [1]. Therefore, searches for such processes are free from irreducible SM backgrounds, and any observation would be an unambiguous signal of Beyond-the-Standard-Model (BSM) phenomena.

The Z boson is a SM particle with well-measured properties and has a high production rate at the LHC. This makes LFV Z boson decays an interesting signal to probe BSM theories with LFV predictions, including models with heavy neutrinos [2], extended gauge [3] or supersymmetry [4].

The most stringent bounds on LFV Z boson decays with a τ-lepton in the final state are set by the LEP experiments: $\mathcal{B}(Z \to e\tau) < 9.8 \times 10^{-6}$ [5] and $\mathcal{B}(Z \to \mu\tau) < 1.2 \times 10^{-5}$ [6]. For the LFV $Z \to e\mu$ decay, the CMS experiment and the ATLAS experiment at the LHC have set upper limits at $\mathcal{B}(Z \to e\mu) < 7.3 \times 10^{-7}$ [7] and $\mathcal{B}(Z \to e\mu) < 7.5 \times 10^{-7}$ [8] respectively.
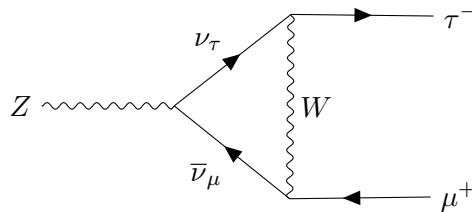
Figure 1: Feynman diagram for the LFV $Z \to \mu\tau$ process in the SM beyond the tree level with neutrino oscillation.

This article presents the searches for the LFV decays of the Z boson into an electron or a muon, hereafter referred to as a light lepton or ℓ, and a hadronically decaying τ-lepton [9] with the ATLAS detector, using pp collisions data with a centre-of-mass energy of 13 TeV.

2 The ATLAS detector

The ATLAS detector [1] [10] at the LHC is a multipurpose particle detector with a forward-backward symmetric cylindrical geometry and a nearly 4π coverage in solid angle. It consists of three major parts:

The inner detector provides precision tracking with silicon pixel and micro strip detectors and additional tracking with a transition-radiation tracker. The inner detector is placed at the centre of the ATLAS detector, surrounded by a superconducting solenoid that provides a 2 T magnetic field.

The electromagnetic and hadronic calorimeters are placed surrounding the solenoid. The electromagnetic calorimeter uses liquid argon and the hadronic calorimeter uses scintillator tiles in the barrel section and liquid argon in the endcaps.

The muon spectrometer is the outermost part of the ATLAS detector. Precise momentum measurements for muons are provided by three layers of tracking chambers and three surrounding large superconducting toroid magnets each containing eight coils.

A two-level trigger system [11] was used during the $\sqrt{s} = 13$ TeV data-taking period, which reduced the recorded event rate to approximately 1 kHz on average.

3 Event selection and classification

3.1 Preselection

Events selected in this analysis are required to have exactly one reconstructed light lepton that passed trigger-matching, isolation and identification criteria [12,13]. The events must also have at least one reconstructed candidate of visible hadronic τ-lepton decay products

---

[1]ATLAS uses a right-handed coordinate system with its origin at the nominal interaction point (IP) in the center of the detector and the z-axis along the beam pipe. The x-axis points from the IP to the center of the LHC ring, and the y-axis points upward. Cylindrical coordinates (r, ϕ) are used in the transverse plane, with ϕ as the azimuthal angle around the beam pipe. The pseudorapidity is defined in terms of the polar angle θ as $\eta = -\ln\tan(\theta/2)$. The transverse momentum and the transverse energy are defined as $p_\mathrm{T} = p\sin\theta$ and $E_\mathrm{T} = E\sin\theta$, respectively.
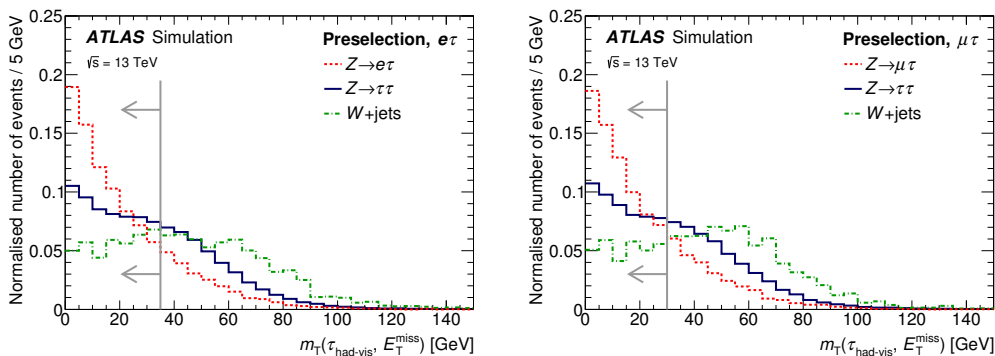
Figure 2: Expected distributions of $m_{\mathrm{T}}(\tau_{\mathrm{had\text{-}vis}}, E_{\mathrm{T}}^{\mathrm{miss}})$ in $Z \to \tau\tau$, W+jets and signal events in the $e\tau$ (left) and $\mu\tau$ (right) channels after preselection requirements. The $Z \to \tau\tau$ and W+jets distributions also include the contributions to fakes from the corresponding processes as predicted by MC simulations. All distributions are normalised to unity.

($\tau_{\mathrm{had\text{-}vis}}$) that passed the "tight" identification criteria [14, 15]. The light lepton and the $\tau_{\mathrm{had\text{-}vis}}$ candidate with leading p_{T} must carry opposite charge. To reduce backgrounds with top quarks, events with b-tagged jets [16] are vetoed. Due to the high $\ell \to \tau$ misreconstruction rates, events with $|\eta(\tau_{\mathrm{had\text{-}vis}})| > 2.2$ (< 0.1) are rejected for the $e\tau$ ($\mu\tau$) channel. The selection described is hereafter referred to as the preselection.

3.2 Signal region

In order to obtain a high signal sensitivity and accurate background estimation, signal region (SR) and calibration regions (CRs) are defined. In the SR, accepted events must satisfy the preselection and two additional selections.

The first selection requires the transverse mass of the $\tau_{\mathrm{had\text{-}vis}}$ candidate and the missing transverse energy $E_{\mathrm{T}}^{\mathrm{miss}}$,

$$m_{\mathrm{T}}(\tau_{\mathrm{had\text{-}vis}}, E_{\mathrm{T}}^{\mathrm{miss}}) \equiv \sqrt{2p_{\mathrm{T}}(\tau_{\mathrm{had\text{-}vis}})E_{\mathrm{T}}^{\mathrm{miss}}\left[1 - \cos(\Delta\phi(\tau_{\mathrm{had\text{-}vis}}, E_{\mathrm{T}}^{\mathrm{miss}}))\right]}, \qquad (1)$$

to be smaller than 35 (30) GeV for the $e\tau$ ($\mu\tau$) channel. The selection can be justified by the fact that the signal events are expected to have $E_{\mathrm{T}}^{\mathrm{miss}}$ from the τ-neutrino in a direction close to the $\tau_{\mathrm{had\text{-}vis}}$ candidate. This results in small $m_{\mathrm{T}}(\tau_{\mathrm{had\text{-}vis}}, E_{\mathrm{T}}^{\mathrm{miss}})$ values. The major backgrounds, W+jets (where jets are misidentified as $\tau_{\mathrm{had\text{-}vis}}$ candidates) and $Z \to \tau\tau$ events, are expected to have higher $m_{\mathrm{T}}(\tau_{\mathrm{had\text{-}vis}}, E_{\mathrm{T}}^{\mathrm{miss}})$ values. The selection is illustrated in Figure 2.

The second selection requires events in which the $\tau_{\mathrm{had\text{-}vis}}$ candidate has one associated track (1-prong $\tau_{\mathrm{had\text{-}vis}}$) to pass cuts on the measured visible invariant mass, $m(\tau\,\mathrm{track}, \ell)$ or $m(\tau_{\mathrm{had\text{-}vis}}, \ell)$, to reject $Z \to \ell\ell$ events with a light lepton misidentified as a $\tau_{\mathrm{had\text{-}vis}}$ candidate. The visible invariant mass $m(\tau\,\mathrm{track}, \ell)$ is reconstructed using the momentum of the track associated to the $\tau_{\mathrm{had\text{-}vis}}$ candidate as measured by the inner detector, While $m(\tau_{\mathrm{had\text{-}vis}}, \ell)$ is reconstructed using energy deposit of the $\tau_{\mathrm{had\text{-}vis}}$ candidate in the calorimeters. The requirements are $m(\tau\,\mathrm{track}, \ell) > 105$ GeV and $m(\tau\,\mathrm{track}, \ell) < 84$ GeV (80 GeV) if $|\eta(\tau_{\mathrm{had\text{-}vis}})| < 2.0$ (> 2.0). Furthermore, events that satisfies 80 GeV $< m(\tau_{\mathrm{had\text{-}vis}}, \ell) <$ 100 GeV must have $m(\tau\,\mathrm{track}, \ell) > 40$ GeV. The selection is illustrated in Figure 3.
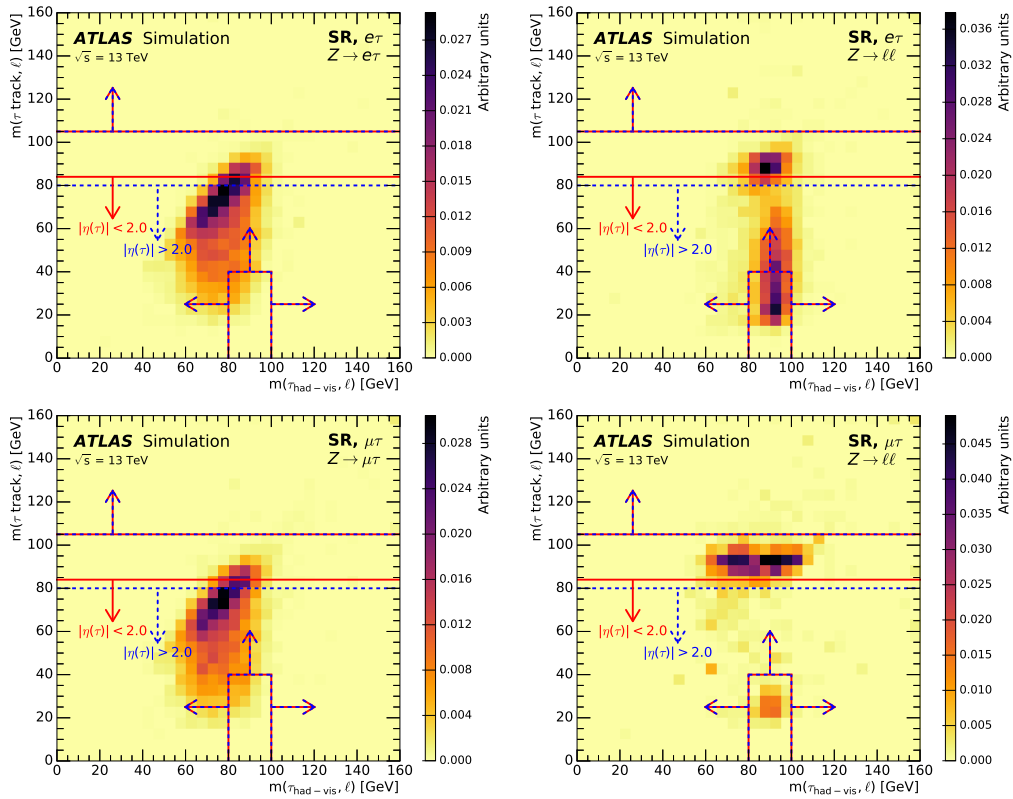
Figure 3: Expected distributions of $m(\tau\ \text{track}, \ell)$ versus $m(\tau_{\text{had-vis}}, \ell)$ in signal (left) and $Z \to \ell\ell$ (right) events with 1-prong $\tau_{\text{had-vis}}$ candidates in the $e\tau$ (top) and $\mu\tau$ (bottom) channels after the SR selection except for the cuts on these two variables.

3.3 Event classification

Events in the SR are classified using neural network (NN) classifiers. Two binary classifiers, the "Z classifier" and the "W classifier", are trained to discriminate signal events from the two major backgrounds, $Z \to \tau\tau$ and W+jets, respectively. Additionally, for events with 1-prong $\tau_{\text{had-vis}}$ candidates, a "Zll classifier" is trained to discriminate signal events from $Z \to \ell\ell$ events. The classifiers are trained separately for the $e\tau$ and $\mu\tau$ channels. The NNs are trained using simulated events passing the preselection but with the $\tau_{\text{had-vis}}$ identification criteria loosen to increase the training sample size. Moreover, for the signal–$Z \to \ell\ell$ classifier, only simulated events with a true light lepton misreconstructed as a $\tau_{\text{had-vis}}$ candidate are used. The 4-momenta of the reconstructed light lepton, $\tau_{\text{had-vis}}$ candidate and $E_{\text{T}}^{\text{miss}}$ are used as input variables to the NNs. In addition, two high-level kinematic variables are also directly inputted to the NNs, including the collinear mass

$$m_{\text{coll}} \equiv \sqrt{2p_{\text{T}}(\ell)\left(p_{\text{T}}(\tau_{\text{had-vis}}) + E_{\text{T}}^{\text{miss}}\right)\left(\cosh \Delta\eta(\ell, \tau_{\text{had-vis}}) - \cos \Delta\phi(\ell, \tau_{\text{had-vis}})\right)}, \quad (2)$$

and $\Delta\alpha$ [17]:

$$\Delta\alpha = \frac{1}{2}\frac{m_Z^2 - m_\tau^2}{p(\tau_{\text{had-vis}}) \cdot p(\ell)} - \frac{p_{\text{T}}(\ell)}{p_{\text{T}}(\tau_{\text{had-vis}})}, \quad (3)$$

where $p(\tau_{\text{had-vis}})$ and $p(\ell)$ are the 4-momenta of the $\tau_{\text{had-vis}}$ and light-lepton candidates respectively, and m_Z and m_τ are the known rest masses of the Z boson and the τ-lepton. For the signal–$Z \to \ell\ell$ classifier, it is found that the visible invariant mass $m(\tau_{\text{had-vis}}, \ell)$ is also an effective input variable and is also used. The inputs are preprocessed by boosting and rotating the ℓ–$\tau_{\text{had-vis}}$–$E_{\text{T}}^{\text{miss}}$ system to remove degeneracy from known symmetries.

The outputs of the different NN classifiers are combined into a final discriminant that is effective in discriminating the signal events from all the major backgrounds. For events with $\tau_{\text{had-vis}}$ candidates that have three associated tracks (3-prong $\tau_{\text{had-vis}}$), the outputs of the Z and W classifiers, X_{Z} and X_{W}, are combined as one subtracted by the normalised distance in the X_{Z}–X_{W} plane from the most signal-like point $(X_{\text{Z}} = 1, X_{\text{W}} = 1)$:

$$\text{NN output (comb)} \equiv 1 - \sqrt{\frac{(1 - X_{\text{Z}})^2 + (1 - X_{\text{W}})^2}{2}}. \quad (4)$$

Similarly, for events with 1-prong $\tau_{\text{had-vis}}$ candidates,

$$\text{NN output (comb)} \equiv 1 - \sqrt{\frac{(1 - X_{\text{Z}})^2 + (1 - X_{\text{W}})^2 + (1 - X_{\text{Zll}})^2}{3}}, \quad (5)$$

where X_{Zll} is the output of the Zll classifier.

4 Background estimation

The backgrounds are estimated using a combination of Monte Carlo (MC) simulations and data-driven techniques. MC simulations are used to estimate background events in which the $\tau_{\text{had-vis}}$ candidate originates from a true lepton, such as $Z \to \tau\tau$, $t\bar{t}$ and diboson events. For events in which a jet is misidentified as a $\tau_{\text{had-vis}}$ candidate ("fakes"), such as W+jets and QCD multijet events, a data-driven method known as the fake factor (FF) method is used.

Table 1: Calibration regions used to derive fake factors. Differences from the SR selection are listed.

CR	Change relative to SR selection
W+jets	$m_\mathrm{T}(\ell, E_\mathrm{T}^\mathrm{miss}) > 40$ GeV and
	$m_\mathrm{T}(\tau_\mathrm{had\text{-}vis}, E_\mathrm{T}^\mathrm{miss}) > 35(30)$ GeV in $e\tau$ $(\mu\tau)$ events
$Z \to \ell\ell$	Two same-flavour opposite-charge light leptons with $81 < m_{\ell\ell} < 101$ GeV
top	$N_{b\text{-jets}} \geq 2$
QCD	Inverted light-lepton isolation

4.1 The fake factor method

In order to estimate backgrounds with fakes, the fake factor method is used. Four fakes-enriched CRs are defined as described in Table 1, from which four fake factors, $F_{W+\mathrm{jets}}$, F_top, $F_{Z \to \ell\ell}$ and F_QCD, are measured, each corresponds to a physical process as indicated in the subscripts.

In each CR, the corresponding fake factor is measured in data as the ratio of the number of events where the $\tau_\mathrm{had\text{-}vis}$ candidate passes the tight identification criteria to that fails the criteria. The fake factor is measured in bins of $p_\mathrm{T}(\tau_\mathrm{had\text{-}vis})$ and $p_\mathrm{T}(\tau \text{ track})$. Contributions from background processes that are not the corresponding target process of the CR or from events where the $\tau_\mathrm{had\text{-}vis}$ candidate does not originate from a jet are estimated by MC simulations and are subtracted from data for the calculation of the fake factors. The fake factors are then combined into a weighted average F, where the individual fake factors are weighted by the fraction of expected contribution from the corresponding process to the total fakes in the SR as predicted by MC simulations. The total yield of fakes in the SR is then estimated by multiplying F to the observed number of events in the SR where the $\tau_\mathrm{had\text{-}vis}$ candidate fails the tight identification criteria.

4.2 Normalisation of major backgrounds

To reduce theoretical uncertainties, the $Z \to \tau\tau$, $Z \to \ell\ell$ and fakes backgrounds are all normalised to data. The $Z \to \ell\ell$ background is normalised to data in a control region with over 99% purity. The normalisation of the $Z \to \tau\tau$ and fakes backgrounds are fit to data simultaneously in a binned maximum-likelihood fit as described in Section 5.

5 Results and interpretations

In order to extract evidence of signal events or set upper limit to the LFV branching ratios, binned maximum-likelihood fits to the combined NN output distribution of data are performed. Free parameters of the fit include the LFV decay branching ratio $\mathcal{B}(Z \to \ell\tau)$ and the normalisations of the $Z \to \tau\tau$ and fakes backgrounds. Systematic uncertainties, including uncertainties in reconstruction, identification and isolation efficiencies, as well as statistical and theoretical uncertainties in the predicted number of events are incorporated in the fit as nuisance parameters with Gaussian or Poisson constraints. The fits are performed separately for the $e\tau$ and $\mu\tau$ channels, since the corresponding branching ratios are not necessarily correlated. Due to the difference in background compositions, events with 1-prong and 3-prong $\tau_\mathrm{had\text{-}vis}$ candidates are fit separately but simultaneously.

The probability of compatibility between data and the background-plus-signal hypothesis is assessed using the CL_S method [18]. By analysing 36.1 fb^{-1} of pp collision data at a centre-of-mass energy of 13 TeV, no significant excess ($> 3\sigma$) of events above the expected background is found. A slight excess in the $e\tau$ channel is observed with significance 2.3σ. The resulting observed (expected) exclusion upper limits at 95% confidence level are $\mathcal{B}(Z \to e\tau) < 5.8 \times 10^{-5}$ (2.8×10^{-5}) and $\mathcal{B}(Z \to \mu\tau) < 2.4 \times 10^{-5}$ (2.4×10^{-5}). The observed and best-fit expected distributions of the combined NN output distributions are shown in Figure 4.

The result of the $\mu\tau$ channel is combined with previous result published by ATLAS with pp collision data at a centre-of-mass energy of 8 TeV [19]. With a combined fit, the observed (expected) exclusion upper limit at 95% confidence level are set at $\mathcal{B}(Z \to \mu\tau) < 1.3 \times 10^{-5}$ (1.8×10^{-5}).

6 Conclusion

Direct searches for LFV decays of the Z boson into a light lepton and a hadronically decaying τ-lepton are presented. Events that exhibits the expected characteristics of the signal events are selected and are discriminated from backgrounds using NN classifiers. The expected NN output distributions are fit to data to quantify the probability of compatibility between data and the background-plus-signal hypothesis, and set exclusion upper limit on the LFV branching ratios. No significant excess of events above the expected backgorund is observed and the upper limits at 95% confidence level are set: $\mathcal{B}(Z \to e\tau) < 5.8 \times 10^{-5}$ and $\mathcal{B}(Z \to \mu\tau) < 2.4 \times 10^{-5}$. When combined with previous published ATLAS results, the upper limit $\mathcal{B}(Z \to \mu\tau) < 1.3 \times 10^{-5}$ is set. The obtained limit is close to the current most stringent limit from LEP experiment: $\mathcal{B}(Z \to \mu\tau) < 1.2 \times 10^{-5}$.

Acknowledgements

We thank CERN for the very successful operation of the LHC, as well as the support staff from our institutions without whom ATLAS could not be operated efficiently.

We acknowledge the support of ANPCyT, Argentina; YerPhI, Armenia; ARC, Australia; BMWFW and FWF, Austria; ANAS, Azerbaijan; SSTC, Belarus; CNPq and FAPESP, Brazil; NSERC, NRC and CFI, Canada; CERN; CONICYT, Chile; CAS, MOST and NSFC, China; COLCIENCIAS, Colombia; MSMT CR, MPO CR and VSC CR, Czech Republic; DNRF and DNSRC, Denmark; IN2P3-CNRS, CEA-DRF/IRFU, France; SRNSFG, Georgia; BMBF, HGF, and MPG, Germany; GSRT, Greece; RGC, Hong Kong SAR, China; ISF, I-CORE and Benoziyo Center, Israel; INFN, Italy; MEXT and JSPS, Japan; CNRST, Morocco; NWO, Netherlands; RCN, Norway; MNiSW and NCN, Poland; FCT, Portugal; MNE/IFA, Romania; MES of Russia and NRC KI, Russian Federation; JINR; MESTD, Serbia; MSSR, Slovakia; ARRS and MIZŠ, Slovenia; DST/NRF, South Africa; MINECO, Spain; SRC and Wallenberg Foundation, Sweden; SERI, SNSF and Cantons of Bern and Geneva, Switzerland; MOST, Taiwan; TAEK, Turkey; STFC, United Kingdom; DOE and NSF, United States of America. In addition, individual groups and members have received support from BCKDF, the Canada Council, CANARIE, CRC, Compute Canada, FQRNT, and the Ontario Innovation Trust, Canada; EPLANET, ERC, ERDF, FP7, Horizon 2020 and Marie Skłodowska-Curie Actions, European Union; Investissements d'Avenir Labex and Idex, ANR, Région Auvergne and Fondation Partager le Savoir, France; DFG and AvH Foundation, Germany; Herakleitos, Thales and Aristeia
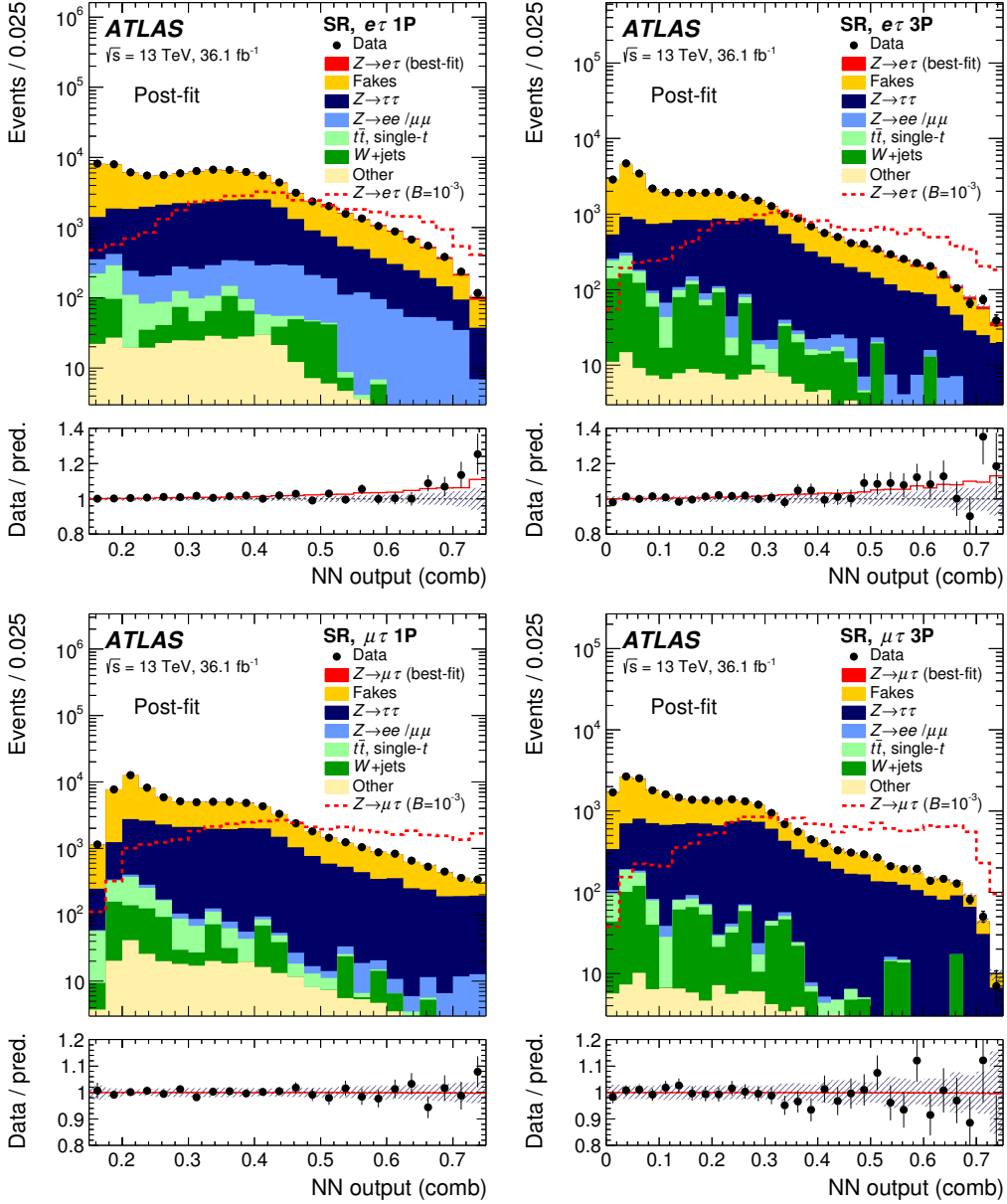
Figure 4: Observed and best-fit expected distributions of the combined NN output in SR for the $e\tau$ (top) and $\mu\tau$ (bottom) channels, for events with 1-prong (left) and 3-prong (right) $\tau_{\mathrm{had\text{-}vis}}$ candidates. The filled histogram stacked on top of the backgrounds represents the signal normalised to the best-fit $\mathcal{B}(Z \to \ell\tau)$. The overlaid dashed line represents the expected distribution for the signal normalized to $\mathcal{B}(Z \to \ell\tau) = 10^{-3}$. In the panels below each plot, the ratios of the observed data (dots) and the post-fit background plus signal (solid line) to the post-fit background are shown. The hatched error bands represent the combined statistical and systematic uncertainties. The first and last bins include underflow and overflow events, respectively.

programmes co-financed by EU-ESF and the Greek NSRF; BSF, GIF and Minerva, Israel; BRF, Norway; CERCA Programme Generalitat de Catalunya, Generalitat Valenciana, Spain; the Royal Society and Leverhulme Trust, United Kingdom.

The crucial computing support from all WLCG partners is acknowledged gratefully, in particular from CERN, the ATLAS Tier-1 facilities at TRIUMF (Canada), NDGF (Denmark, Norway, Sweden), CC-IN2P3 (France), KIT/GridKA (Germany), INFN-CNAF (Italy), NL-T1 (Netherlands), PIC (Spain), ASGC (Taiwan), RAL (UK) and BNL (USA), the Tier-2 facilities worldwide and large non-WLCG resource providers. Major contributors of computing resources are listed in Ref. [20].

References

[1] J. I. Illana, M. Jack and T. Riemann, *Predictions for $Z \to \mu\tau$ and related reactions*, In *5th Workshop of the 2nd ECFA - DESY Study on Physics and Detectors for a Linear Electron - Positron Collider Obernai, France, October 16-19, 1999*, pp. 490–524 (1999).

[2] J. I. Illana and T. Riemann, *Charged lepton flavor violation from massive neutrinos in z decays*, Phys. Rev. D **63**, 053004 (2001), doi:10.1103/PhysRevD.63.053004.

[3] T. K. Kuo and N. Nakagawa, *Lepton-flavor-violating decays of Z^0 and τ*, Phys. Rev. D **32**, 306 (1985), doi:10.1103/PhysRevD.32.306.

[4] F. Gabbiani, J. H. Kim and A. Masiero, *$Z^0 \to b\bar{s}$ and $Z^0 \to \tau\mu$ in SUSY: Are they observable?*, Physics Letters B **214**(3), 398 (1988), doi:10.1016/0370-2693(88)91384-6.

[5] OPAL Collaboration, *A search for lepton flavour violating Z^0 decays*, Zeitschrift für Physik C Particles and Fields **67**(4), 555 (1995), doi:10.1007/BF01553981.

[6] DELPHI Collaboration, *Search for lepton flavour number violating Z^0-decays*, Zeitschrift für Physik C Particles and Fields **73**(2), 243 (1997), doi:10.1007/s002880050313.

[7] CMS Collaboration, *Search for Lepton Flavor Violation in Z and Higgs decays with the CMS Experiment*, Nuclear and Particle Physics Proceedings **287-288**, 160 (2017), doi:10.1016/j.nuclphysbps.2017.03.067, The 14th International Workshop on Tau Lepton Physics.

[8] ATLAS Collaboration, *Search for the lepton flavor violating decay $Z \to e\mu$ in pp collisions at $\sqrt{s} = 8$ TeV with the atlas detector*, Phys. Rev. D **90**, 072010 (2014), doi:10.1103/PhysRevD.90.072010.

[9] ATLAS Collaboration, *A search for lepton-flavor-violating decays of the Z boson into a τ-lepton and a light lepton with the ATLAS detector* (2018), `https://arxiv.org/abs/1804.09568`.

[10] ATLAS Collaboration, *The ATLAS experiment at the CERN Large Hadron Collider*, JINST **3**, S08003 (2008), doi:10.1088/1748-0221/3/08/S08003.

[11] ATLAS Collaboration, *Performance of the ATLAS Trigger System in 2015*, Eur. Phys. J. C **77**, 317 (2017), doi:10.1140/epjc/s10052-017-4852-3.

[12] ATLAS Collaboration, *Electron efficiency measurements with the ATLAS detector using the 2015 LHC proton–proton collision data*, ATLAS-CONF-2016-024 (2016), `https://cds.cern.ch/record/2157687`.

[13] ATLAS Collaboration, *Muon reconstruction performance of the ATLAS detector in proton–proton collision data at $\sqrt{s} = 13$ TeV*, Eur. Phys. J. C **76**, 292 (2016), doi:10.1140/epjc/s10052-016-4120-y.

[14] ATLAS Collaboration, *Reconstruction, energy calibration, and identification of hadronically decaying tau leptons in the ATLAS experiment for Run-2 of the LHC*, ATL-PHYS-PUB-2015-045 (2015), `https://cds.cern.ch/record/2064383`.

[15] ATLAS Collaboration, *Measurement of the tau lepton reconstruction and identification performance in the ATLAS experiment using pp collisions at $\sqrt{s} = 13$ TeV*, ATLAS-CONF-2017-029 (2017), `https://cds.cern.ch/record/2261772`.

[16] ATLAS Collaboration, *Optimisation of the ATLAS b-tagging performance for the 2016 LHC Run*, ATL-PHYS-PUB-2016-012 (2016), `https://cds.cern.ch/record/2160731`.

[17] S. Davidson, S. Lacroix and P. Verdier, *LHC sensitivity to lepton flavour violating Z boson decays*, JHEP **09**, 092 (2012), doi:10.1007/JHEP09(2012)092.

[18] A. L. Read, *Presentation of search results: the CL_s technique*, J. Phys. G **28**, 2693 (2002), doi:10.1088/0954-3899/28/10/313.

[19] ATLAS Collaboration, *Search for lepton-flavour-violating decays of the Higgs and Z bosons with the ATLAS detector*, Eur. Phys. J. C **77**, 70 (2017), doi:10.1140/epjc/s10052-017-4624-0.

[20] ATLAS Collaboration, *ATLAS computing acknowledgements 2016–2017*, ATL-GEN-PUB-2016-002, `https://cds.cern.ch/record/2202407`.